Vol. 45, No. 3 (2023) 542-560, DOI: 10.24874/ti.1463.03.23.06

Tribology in Industry

www.tribology.rs

REVIEW

Numerical and Experimental Studies on Performance Enhancement of Thrust Pad Bearing Employing Surface Texture: A Review

Dhanishta Sirohi[a,*] and Shipra Aggarwal[a]

[a]*Deptt. Of Mechanical and Automation Engineering, Indira Gandhi Delhi Technical University for Women, Kashmere Gate, Delhi.*

Keywords:

Hydrodynamic lubrication
Laser surface texturing
Thrust pad bearing
Cavitation
Load carrying capacity
Coefficient of friction

* Corresponding author:

Dhanishta Sirohi
E-mail: dhanishta.sirohi07@gmail.com

Received: 20 March 2023
Revised: 22 April 2023
Accepted: 13 June 2023

A B S T R A C T

This article aims to review the research findings in the field of surface texture on fixed pads, tilting pad thrust bearings and sliders. Numerical/computational and experimental explorations have been done by researchers to improve the performance behaviours by varying texture parameters such as the shape of texture, its depth, width, texture area density, location and extent. Articles are classified as experimental and numerical techniques which are further categorized depending on the inclusion of cavitation and thermal effects. There are indications that the presence of texture (comprising of pits, dimples grooves and pockets) on the pad surface results in a reduction of the coefficient of friction and enhancement of load-carrying. The presence of a pocket is more beneficial in terms of increasing the minimum film thickness and decreasing the coefficient of friction than a pad with dimples or grooves. It is also observed that self-adaptive and bionic textures improve the performance behaviour of thrust pad bearings in comparison to conventional textures.

1. INTRODUCTION

Thrust pad bearings are used to withstand and guide the thrust or axial loads in hydraulic machinery, helical gearboxes and generators due to high load-carrying capacity (LCC), low friction and good damping tendency [1]. In the past, researchers have employed different techniques, such as surface texture and surface profiling on pads, and used different types of lubricant additives to improve the performance of thrust pad bearings. Surface texture is used broadly to enhance the performance behaviour of thrust pad bearing [2,3]. Texture act as numerous small hydrodynamic bearings that withstands load and reduces surface wear, behave as a small pool of oil and transfer lubricating oil to the rubbing surface and can corner the wear debris during the operation [4]. It has also been observed that different surface textures (dimples, pockets, pits, pores, and grooves) decrease friction coefficient,

enhance LCC and increase minimum film thickness. A schematic illustration of different micro-geometries comprising surface texture is shown in Fig. 1.

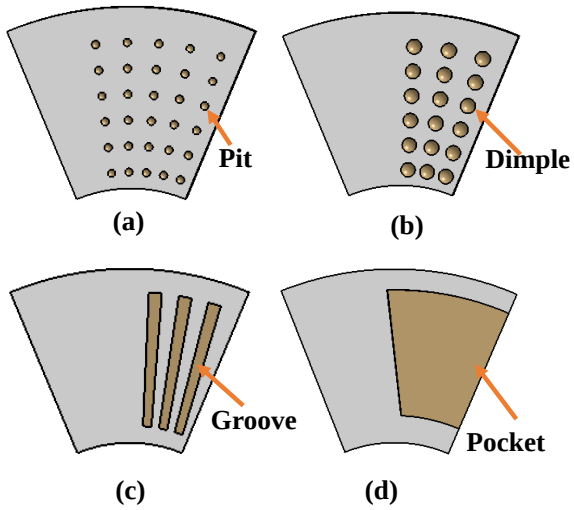

Fig. 1. Different types of micro-geometries comprising texture (a) pits (b) dimples (c) grooves (d) pocket.

These micro-geometries are mainly classified according to their dimensions such as depth, diameter, shape, etc. which are discussed in detail in subsequent sections. It has been observed that the texture parameters such as the number of textures, texture area density, depth of texture, aspect ratio of pad and convergence ratio affect the performance behaviour of bearings [5]. In the past researchers working on textured bearing neglected cavitation and assumed pressure not to reach the sub-ambient zone. However, it is revealed that it is necessary to include thermal effects [6], and mass-conserving cavitation effects [7] to get a realistic solution. Recently, it has been perceived by researchers [8] that from nature, many bionic textures can be developed and can have many applications in engineering. Bionic textures designs are taken from biological organisms or adopted from nature. Reduction in drag, friction and wear and enhancement in LCC and minimum film thickness by the presence of bionic textures on the surface have also been reported [8]. Xie et al. [9] discussed the lubrication regime, thermal effects and tribological behaviours of water-lubricated bearings. A new type of texture is introduced by researchers [10,11] which can deform at micro or nano scale at increasing applied load in order to support that load successfully and maintain constant film thickness called self-adaptive dimples/ grooves. However, work done on self-adaptive [10,11] and bionic texture [8,9] on fixed pad thrust bearings is limited. A schematic representation of bionic and self-adaptive texture is shown in Fig. 2.

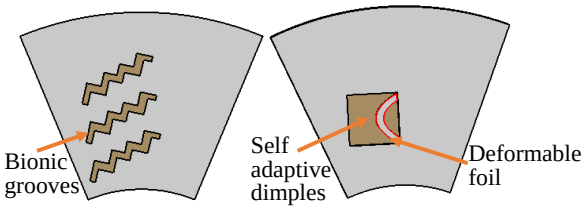

Fig. 2. Schematic diagram of (a) bionic texture (b) self-adaptive texture.

This article presents research findings in the field of texture on parallel sliders, parallel thrust bearings, inclined thrust pad bearings, tilted thrust pad bearings and tribometers. The articles are classified based on the research method employed and categorized into two types, namely,

- experimental studies and
- numerical/ computational studies.

Articles involving numerical methods are further classified into four categories, namely,

- isothermal studies without considering cavitation effects,
- isothermal studies incorporating mass conserving algorithm,
- numerical studies incorporating thermal effects without considering cavitation, and
- numerical/computational studies considering thermal and cavitation effects.

This classification is illustrated in Fig.3. Sixty per cent of the research has been done theoretically using numerical/ computational methods. Out of which, around 16% of research is done by numerical studies incorporating thermal effects published during the last 25 years. The distribution of articles in different categories is shown in Fig. 4.

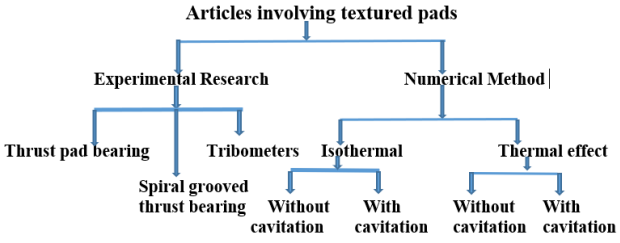

Fig. 3. Classification of literature review.

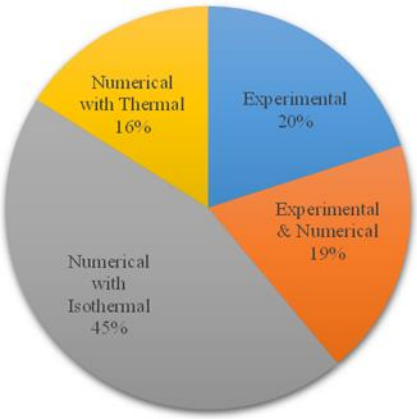

Fig. 4. Categories of research articles based on solution methodology.

2. EXPERIMENTAL STUDIES

Research has been done by conducting experiments in the field of surface texture on thrust pad bearing [12-21], spiral groove thrust pad bearings [22-26] and different contact configurations in tribometers [3,11,27-41].

The performance of the bearing is measured in terms of LCC, coefficient of friction and minimum film thickness. It is shown that the performance of the bearing is improved in the presence of texture comprising of micro geometries such as dimples, pits, grooves and pockets. Texture parameters such as number, shape of texture, depth, width, texture area density, location and extent affect the performance behaviour of the bearing. These texture parameters are also influenced by the bearing's geometry (convergence ratio and aspect ratio) and operating conditions (speed and load).

2.1 Thrust pad bearing

A thrust pad bearing is used in machinery to support the axial load and decrease friction. The function of the thrust bearing is to control rotation between parts, prevent the shaft from moving in the axial direction, and transfer thrust and load applied on the shaft, as shown in Fig 5. Research is being carried out to improve the performance with regard to enhancing load and decreasing the friction of the thrust pad bearing. Experimentally research was done on parallel slider bearing [12-15], thrust pad bearing [16-20] and tilted thrust bearings [21] operating under applied load varying from 5-2548 N [12-21] and speed from 200-12000 rpm [12-21]. The friction coefficient and LCC are affected by texture area density [15,17-18], depth [13,17-19], width [19], texture circumferential extent [15,19], texture radial extent [15,19], texture position [14,17] and different shape of dimple such as circular [14,19] and rectangular [14,17]. These experimental studies' results revealed that friction coefficient and LCC are affected by high speed [12, 14-15, 19-20]. The centrifugal force increases gradually at high speed, which reduces bearing clearance so more fluid is squeezed away from the bearing land portion and increases the shear rate of the film, which may cause high friction torque [12].

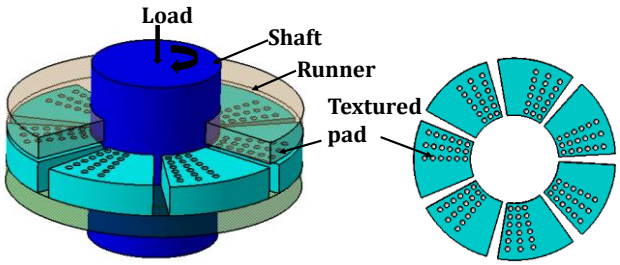

Fig. 5. Textured thrust pad bearing.

It has also been observed that the friction coefficient of untextured bearing is higher than partial textured bearing over the entire load range [12, 14]. High friction of untextured bearing is due to smaller clearance of bearing which results in high viscous shear [12]. Henry et al. [17] suggested that pocket has a favourable effect on friction reduction compared to textured and taper land under the same operating condition. It is also noticed that LCC is affected by the space between adjacent circular grooves [19]. Both experimental and theoretical methods show that partial texture improves bearing performance more than full texture [19]. A schematic diagram of partial and full-textured pads is illustrated in Fig. 6.

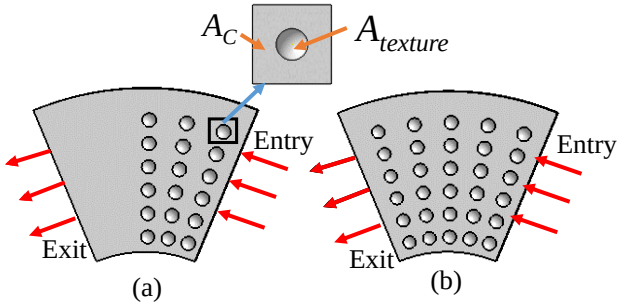

Fig. 6. Schematic representation of (a) partial texture towards the entry side (b) full texture.

Table 1. Articles involving the study of thrust-bearing texture by experimental research.

Article	Input parameters	Findings
Mikula [21] 1985	Leading edge groove shoe design. N: 4000 – 12000 rpm	Operate at 75% less oil flow rate. Temperature reduced by 20% at 12000 rpm
Etsion et al. [12] 2004	SiC disks, circular dimples Unidirectional and bidirectional partial laser surface texturing N: 1500-3000 rpm, W_a: 0-500 N	μ: 0.01 for textured and 0.025 for untextured at 460 N and 1500 rpm h_{min}: 6 μm for textured, 1.7 μm for untextured
Glavatskih et al. [16] 2005	Thrust bearing test rig, grooves d: < 10 μm, N: 500; 3000 rpm P_a: 0.5-2.0 MPa	μ reduced by 10%
Kawabata [13] 2012	Reciprocating friction sliding test, circular dimples, D: 4; 5; 5.5 μm, N_d: 176; 118; 106 d: 0.5-30 μm	d nearly equal to h_{min} obtained: Maximum W, Minimum μ.
Henry et al. [17] 2015	Thrust bearing test rig, dimples W_a:1000-5000 N; d: 20 mm; ρ_c: 16%; 25% and 56% Two configurations: Inlet and centred in the cells	W increased: ρ_c of 56%, Low load range. 24K less temperature compared to untextured. Inlet texture improves bearing performance as compared to centred.
Henry et al. [18] 2015	Thrust bearing test rig, pocket N: 0-2000 rpm, W_a: 750-2000 N Untextured parallel surface, Taper land, Pocketed, Textured parallel surface	Pocketed land thrust bearing: Best geometry, Avoid wear Minimize friction
Miyanaga et al. [14] 2020	Rotating disk test, Dimples Shape: Circular, Transverse rectangular, Longitudinal rectangular N: 0-600 rpm	N: 600 rpm T_f is lowest in circular dimples
Changsheng et al. [15] 2021	Rotor-bearing test, circular dimples N: 1200-2400 rpm, W_a: 1000-2500 N	Damping is higher at high speed and low load than no texture bearing.
Chen et al. [19] 2021	Friction and wear testing machine, circular grooves, d: 0-40 μm, w: 100-2500 μm, N: 200-600 rpm, W_a: 15 N; 45 N, β: 0-1, α: 0-1	Partial texture improves performance more than full texture. Optimum α is 0.8–0.9, Optimum w_r and d_r is 5 Experimental result agrees with theoretical at high rotational speed, low load conditions.
Bouyer et al. [20] 2021	Thrust bearing test rig, Circular pocket N: 0-8000 rpm, W_a: 1000 N and 1500 N d: 0.4 mm, D: 6 mm	Hydrostatic lift pockets: Reduced W, Thermal deformations T_f is 1.6 Nm at 1000 N and 3.0 Nm at 1500 N flat land with pocket

It can be seen that dimples are located towards the entry side in the partial-textured pad and over the entire surface in the full-textured pad as shown in Fig. 6. A summary of articles involving the study of textured thrust-bearing by experimental research is given in Table 1.

From Table 1, it can be noticed that laser surface texturing is mostly used by researchers [12,14,17,19] to generate texture on pad surfaces. Pocketed surfaces result in lower friction compared to other textured surfaces [18]. A partially textured pad surface improves performance more than a full textured pad surface [12,17,19]. The position of the dimple at the inlet of the cell [17] improves performance as compared to the centre of the cell. Thermal deformation of the pad reduced LCC [17,20]. The performance of the bearing is improved when the texture radial extent is in the range of 0.8-0.9 [19] and the depth of dimples equals to minimum film thickness [13].

2.2 Spiral groove thrust bearing

Water-lubricated spiral groove bearings can withstand high loads for rotary machines, however, at higher speeds, friction loss increases [22]. Research shows that modified conventional spiral grooves can reduce power loss at high speed [22-23]. Researchers have used spiral groove bearing [22-26] to investigate the performance of bearings at an applied load of 45-250N [22-26] and operating speed of 20-2700 rpm [22-26]. Bearing performance parameters are affected by speed [22-25], load [24-26], aspect ratio [22], depth of grooves [22,24,26] and texture area density [26]. Fesanghary et al. [22] suggested that LCC depends on the texture aspect ratio. A summary of articles involving the study of spiral grooved thrust bearing by experimental research is given in Table 2.

Table 2. Articles involving the study of spiral grooved thrust bearing by experimental research

Article	Input parameters	Findings
Fesanghary et al. [22] 2013	Radius ratio=outer radius/inner radius: 1.2-3.5 W_a: 0-45 N, N: 100-300 rpm Laser surface texturing	Optimum groove increases W up to 14–36% for a 2.5 radius ratio.
Ibrahim et al. [23] 2018	Spiral design and modified spiral design compared with the seal, N_g: 12, d: 5 µm Modified spiral groove no.: 24, Depth: 8 µm,	Leakage decreases as speed of rotor increases. Modified spiral reduces air leakage.
Hu et al. [24] 2019	N: 20-1000 rpm, W_a: 100-200 N, N_g: 12 d: 3 µm	T_f increases proportionally with the W_a. W increases proportionally with N. Pressure and cavitation area change rapidly during the start-up period at 100N load.
Lin et al. [26] 2022	Water lubricated bearing, N_g: 12 d: 0-100 µm, W_a: 50-250 N N: 1500; 1800; 2100 rpm, ρ_c: 0; 9; 15; 25% Laser surface texturing	W of the textured bearing increases by 13.8% when: h_{min} is 25 µm, d_g = 50 µm Reduction of 7.1% T_f when h_{min} is 10 µm, ρ_c is 25% For maximum W, d_r = 2
Xianming Gan [25] 2021	Water lubricated bearing N: 900-2700 rpm, W_a: 10-90 N, N_g: 12, d: 40 µm	T_f is 42.5 Nmm at 2700 rpm and 90 N, 36 Nmm at 900 rpm and 90 N

From Table 2, it can be seen that modified spiral grooves can improve the performance of bearings as compared to conventional grooved bearings [22-23]. The friction torque of the bearing increases proportionally with the applied load [24-25].

2.3 Tribometers

Different contact configurations such as cylindrical and spherical disk specimens [27-29], cylindrical on flat test geometry [30], pin on disk [31-35], reciprocating friction test rig [36], rectangular bar specimen [37], ring type specimen [3,38-41], ball on three flat [42] were used by the researchers to find the performance of the textured surface. Ball on three flat contact geometry used by Hsu et al. [42] concluded that the presence of large-sized dimples reduced friction in hydrodynamic lubrication. In contrast, small-sized dimples reduced friction in mixed lubrication. Different shapes of dimples such as droplets, parallelograms, mixtures (by combining two different shapes) and overlaps (by laying one shape over the other) were used. Mixture and overlap design provided friction coefficients less than 0.01 at 157 MPa and 0.055 at 470 MPa respectively [42]. In cylindrical and spherical disk, the cylinder is rotating with a speed in the range of 200-1200 rpm [27-29]. Load is applied on disk in the range of 98-3000 N [27-29] and the face of the disk is textured. A cylinder on flat test geometry is a modified pin on the disk tester. In this setup, the textured disk is rotating and load is applied to the cylinder [30]. The result shows that LCC is affected by the size of the dimple and the radius of the cylinder [30]. The reciprocating friction test rig consists of upper specimen textured with different shapes of grooves in face-to-face contact with the lower specimen under the applied load [36]. Block-on-ring test rig thrust specimens resemble annular rings [39].

The researchers have taken bionic texture from animals such as sharks [31], fish [8], frogs [35] and bush crickets [35]. The result of these experiment set up reveals that LCC is affected by texture area density [3,27-29, 35- 36,40], speed [27,34,39,41], applied load [41], depth of texture [3,28-29,31,34,36], the shape of dimple such as rhombus [31], round [35], hexagonal [35], elliptical [36] and triangular [41]. Film thickness can be increased by 40% with a texture area density of 39% [40]. Panigrahi et al. [41] suggested that triangular shape dimples provide higher bearing clearance in comparison to circular, elliptical, and square shape dimples in a parallel slider due to additional hydrodynamic lift which causes less shear in the lubricant leading to lesser frictional torque. The lowest friction coefficient is 0.015 obtained on a surface having a texture area density of 8.6% with 0.3m/s speed under contact pressure of 5 MPa [32]. The friction coefficient is not affected by surface roughness in the hydrodynamic regime [39]. A summary of articles involving the study of texture in different contact configurations of tribometers employing experimental research is given in Table 3.

From Table 3, it can be concluded that pits [27-30] have been used less as compared to dimples [32-34, 36, 41]. Small dimples have increased LCC and reduced the coefficient of friction compared to large-sized dimples [30,41]. Laser surface texturing [27] and CNC machines [37] have been used to generate texture on the pad surface. Surface roughness did not affect the coefficient of friction [39].

3. NUMERICAL/COMPUTATIONAL STUDIES

More than sixty per cent of the research has been done using numerical methods. Researchers worked on different types of textures comprising dimples, pockets or grooves. Numerical simulations have been carried out to investigate the effects of texture parameters such as depth of texture, texture area density, convergence ratio of pad and shape of texture on LCC and friction coefficient. Numerical/computational studies can be classified into four categories, namely,

- isothermal studies without considering cavitation effects [10,43-56],
- isothermal studies incorporating mass conserving algorithm [3,11,37,57-69],
- numerical studies incorporating thermal effects without considering cavitation [70-75] and
- numerical studies considering thermal as well as cavitation effects. [2,8,76-80].

3.1 Isothermal studies without considering cavitation effects

Initial investigations were carried out to understand the effects of the presence of surface texture on the performance of the bearing assuming isothermal conditions. Finite difference method (FDM) [10, 43-50] and Finite volume method (FVM) [51-56] were used to solve the numerical model. 2-D Reynolds equation for an incompressible Newtonian fluid in steady-state laminar flow used by the researchers to find bearing performance parameters. Firstly, the Reynolds equation is discretized by FDM and numerically solved for pressure values at different nodes by Gauss Seidal iterative method. In FVM, bearing performance is calculated by computational fluid dynamics simulations which are based on the solution of the Navier-Stokes equation. Research revealed that the performance behaviours of bearing such as LCC are increased by 20% [44] and the coefficient of friction is reduced by more than 44% [50,55]. These performance parameters are affected by types of micro-geometries present in the texture such as dimples [43-44,46-48,53-54,56], grooves [45,52], pockets [51], self-adaptive grooves [10], bionic dimples[49] and parameters of texture such as aspect ratio [43], texture extent along the length of the pad [43,45], depth [43,45-47,49,54,56], width [48,52,54], texture area density [43-44], texture location [45,47,51,53], number of dimples/grooves [45-47], the shape of texture such as elliptical [44], square[45], and cylindrical [52], splined [52] and convergence ratio of pad [46,48,51,53,56]. Zeng et al. [50] obtained the maximum friction reduction of 44% in comparison with the smooth surface for a circular concave texture of depth 20 μm.

The self-adaptive texture surface used by Duvvuru et al. [10] can deform itself into micro or nano grooves over the surface when the applied load is increased. Thin foil was used as a self-adaptive surface. Deformation of the surface depends on material properties, dimensions and lubricant pressure. Beam theory was employed to find the foil deflection. A combination of dimples and grooves suggested by Aggarwal and Pandey [45] revealed that a square cross-sectional shape gives the best results among circular, square, trapezoidal, and triangular grooves. The presence of five square cross-sectional grooves of 60 μm depth placed in the inlet zone yields the best results compared to placing at some other locations on the pad's surface. Placing grooves on the pad surface yields greater improvement in the performance parameters compared to dimples. A summary of articles involving isothermal studies of textures without considering cavitation effects is given in Table 4.

Table 3. Articles involving the study of texture in contact configurations by experimental research.

Article	Contact configurations	Input parameters	Findings
Hsu et al. [42] 2016	Ball on three flat	Self-adaptive dimple U: 0.19-1.34 m/s, P_a: 157-470 MPa Pattern: Droplet, Parallelogram, Mixture (Combination of two shapes), Overlap (Laying one shape over other)	Mixture and overlap designs provided the best performance μ: Less than 0.01 at 157 MPa and 0.055 at 470 MPa.
Wang et al. [27] 2001	Cylindrical, spherical disk	Pits D: 100 µm; 150; 200 µm, W_a: 98-2548 N ρ_c: 0-22.556%, d: 8-11 µm, N: 200-1200 rpm	Increased W by 20% when: ρ_c: 2.8%, N in range of 400-1200 rpm
Wang et al. [28] 2003	Cylindrical, spherical disk	Pits in a square array. N: 400-1200 rpm, W_a: 300-3000 N, ρ_c: 0-5%, D: 0-650 µm, d: 0-3.3 µm	W is 2.5 times over untextured when: D: 350 µm, d: 3.2 µm, ρ_c: 5%
Wang et al. [29] 2008	Cylindrical, spherical disk	Pits D: 0-650 µm, d: 0-3.4 µm ρ_c: 0-5%, N: 400; 800; 1200 rpm	Increased W two times as untextured when: ρ_c: 5%, d/D: 0.015
Wang et al. [30] 2009	Cylindrical on flat test geometry	Pits D: 20; 40; 60 µm, d: 0.6; 1.2; 1.8 µm ρ_c: 7%, U: 0.02-0.2 m/s, W_a: 10-30 N	W increased, μ is reduced using small diameter pits
Lu [31] 2014	Pin on disk	Bionic dimples d_r: 0.25-1.25, w_r: 0-0.85	Sharkskin design: Builds up h_{min}, enhance W, μ < 0.1 with w_r > 0.45.
Zhang et al. [32] 2014	Pin on disk	Dimples Square array, Linear radiating array D: 500; 950; 650; 800 µm, d: 10 µm ρ_c: 10.7; 13.9; 8.6; 11.6%, U: 0.3; 0.6; 0.8 m/s P_a: 2.6 -5 MPa	Lowest μ 0.015 at: ρ_c of 8.6%. D 650 µm at U 0.3 m/s Contact pressure 5 MPa Square array
Ancona et al. [33] 2017	Pin on disk	Dimples W_a: 0.25-1.5 N, ρ_c: 50%, d: 5-25 µm. Shape of the dimple: Elliptical, Rectangular No. of loops in Elliptical: 5; 10; 15; 20; 25 No. of loops in Rectangular: 4; 9; 14; 19; 25	μ rectangular shape dimple 20% less than elliptical shape
Taee et al. [34] 2017	Pin on disk	Dimples W_a: 30; 60 N, U: 0.1; 0.4; 0.7 m/s, d: 3; 5; 15 µm	μ decreases by 12–23% h_{min}, W increased as N increases.
Dai et al. [35] 2020	Pin on disk	Hexagonal dimples: D 200 µm, d 5 µm, ρ_c 50%-80%, Round dimple: D 200 µm, ρ_c 10%-40%	μ enhanced by: Hexagonal dimple patterns, ρ_c 80%.
Yu et al. [36] 2011	Reciprocating friction test rig	Dimples d: 3-18 µm, ρ_c: 2.6%; 10.4%; 15.5%; 22.9% shape: Circle, Square, Ellipse	Elliptical dimples: Largest W. Optimum µ: ρ_c 10.4%, d: 8-10 µm, shape: Elliptical
Mao et al. [37] 2019	Rectangular bar specimen	Dimples Rotational velocity: 30-90 rad/s, d: 0.01-0.08 mm, D: 0.1-0.18 mm.	μ is 0.26 when: D is 0.15-0.16 mm, Rotational velocity is 30 rad/s μ is 0.165 when the d 0.06 mm.
Yagi et al. [38] 2008	Ring type specimen	Pits P_a: 0.2-0.5 MPa,	μ: Less than 0.05 at 0.5 MPa. Greater than 0.1 at 0.2 MPa
Zhang [3] 2012	Ring type specimen	Grooves N_g: 24; 24; 96, d: 4.6 µm; 5.2 µm; 10.2 µm; Cavitation pressure: 10-90 kPa	μ is 71% of the value obtained in the experiment using the JFO model
Hirayama et al. [39] 2015	Ring type specimen	Grooves d: 200 nm, N: 0-600 rpm	h_{min} 200–300 nm, for all experiments. μ is not affected by surface roughness.
Zavos et al. [40] 2018	Ring type specimen	Square Pocket W_a: 5-50 N, N: 0.35-4 m/s Square-shaped pocket: T_1 ρ_c: 9.7%, T_2 ρ_c: 39%	h_{min} increased by 40% with the T_1. T_2 effective to reduce friction and wear than T_1
Panigrahi et al. [41] 2020	Ring type specimen	Dimples shape: Circular, Elliptical, Square, Triangular d: 80; 160; 200 µm, Size: 1100; 2300; 3500 µm, N: 0-900 rpm	Increases T_f as W_a and N increase Decreases h_{min} as W_a and N increase Triangular shape develops more W and more h_{min} as compared to other shapes.

Table 4. Articles involving isothermal studies without considering cavitation effects.

Article	Input parameters	Findings
Brizmer et al. [43] 2003	FDM, Circular dimples, ρ_c: 0-80%, Slider L/B: 0.1-infinite, Dimple extent in sliding direction: 0-1, d_r: 50-200	Full texture is not useful to develop W Maximum W: Dimple extent along sliding direction is 0.6 Slider $L/B \geq 0.5$
Yu et al. [44] 2009	FDM, dimple d: 8 μm, ρ_c: 7%, U: 0.1; 0.2 m/s, Shape of dimple: Ellipse, Circular, Triangle	26.3% W increased by ellipse over circular dimple at 0.2m/s
Aggarwal and Pandey [45] 2012	FDM, grooves d: 10-100 μm,N_g: 0-6 Location of grooves: Inlet, Mid, Outlet, overall Shape: Circular, Square, Triangular, Trapezoidal	Enhancing W and reduced μ by: N_g: 5, d: 60 μm square-shaped grooves placed at the inlet. Grooves improve performance more than dimples
Duvvuru et al. [10] 2008	FDM, self- adaptive grooves Euler Bernoulli beam theory h_{min}: 1; 3; 4; 5; 7; 10 μm Foil thickness:10; 15; 20 μm	W decreases with an increase in h_{min}. Film stiffness and W of self–adaptive surfaces can be greater than conventional surfaces.
Yagi et al. [46] 2017	FDM, circular dimples Balancing wedge action to multiple dimples K: 0-1, d_r: 0.1-10, N_d: 1-100, w_r: 0.2-1	Dimples at the inlet of the pad provides: Maximum W
Kouider et al. [47] 2018	FDM, dimple, grooves N: 500-3000, d: 20; 30; 40 Four types of texture: Circumferential groove, Radial groove, Rectangular dimple, Dimple in the mid of the pad, Position of dimple: Inlet, Middle, outlet	Radial grooves place at inlet yields: Maximum W, Minimum T_f Dimple placed close to pivot position obtained maximum W
Zhang et al. [48] 2019	FDM, circular dimples D: 400 μm, d: 10 μm, K: 0.2; 0.4; 0.8; 1.2, N_d: 0-40, Width of pad: 5; 7; 9; 11 mm	Dimples arranged in Triangular/trapezoid pattern at the inlet of the bearing pad provides: High W, Low μ
Yu et al. [49] 2020	FDM, bionic dimples Grids of dragonfly wings Groove d: 35 μm, Airflow angle: 0-90^0 N: 45,000-90,000 rpm	Airflow angle of 24°: highest W for a circular surface W is 4.69 N At 90,000 rpm which is 46.11% more than conventional grooves.
Zeng et al. [50] 2021	FDM, dimples Circular concave d: 5-30μm Spherical convex height: 3; 5; 7; 15; 20 μm, Spherical convex bottom: 48; 72; 96; 120 μm	44% μ reduced in comparison with the smooth surface at U is 0.8 m/s Circular concave d: 20 μm
Gosman et al. [51] 2005	FVM, square pocket d: 0-40 μm, K: 0.001; 0.01; 0.1; 1	Minimum μ 0.00019 when K is 1
Glavatskih et al. [52] 2005	FVM, grooves Re: 40; 80; 120; 160 Geometry: Cylindrical, Splined w_r: 0.15-0.50, d_r: 0.25-1.25, displacement to width ratio: -0.3; 0; 0.3	Maximum W: d_r: 0.5-0.75 for all geometry and width F reduced: High d_r, High w_r Best performance: cylindrical geometry
Cupillard et al. [53] 2008	FVM, rectangular dimples K: 0-2, Dimple d_r: 0.1; 0.33; 0.75	Maximum W depends on: K, d, inlet position of dimple
Han et al. [54] 2010	FVM, spherical cap micro dimples d_r: 0.5-2.20, w_r: 0.2-0.8, Re: 10; 80; 160	W increases, Increase Re, Increase w_r Maximum W, minimum μ: d_r 0.80–2.00
Charitopoulos et al. [56] 2013	FVM, grooves Wavy parallel slider, Wavy converging B/L: 0.5-infinite, K: 0.75-1.31	Improvement in W 30% wavy parallel slider 15% wavy converging
Sun et al. [55] 2017	FVM, sawtooth riblet dimples h_{min}: 0.3; 0.5; 3 μm, d: 10; 20; 50 μm, U: 0.01; 0.02; 0.03 m/s	Sawtooth riblet can provide: Maximum reduction in μ 93.83% at 0.03m/s.

From Table 4, it can be noticed that texture placed at the inlet [45-46,48,53] is more beneficial than other locations such as the exit [46] and close to the pivot [47] of the pad. Different shapes of dimples and grooves such as circular [43-46], square [45,51], elliptical [44] and cylindrical [52] have been investigated which improves the performance behaviours of bearing. Maximum pressure is generated when the convergence ratio is less than 1 [48] or equal to 1 [51,53]. The performance of the bearing is improved when the depth ratio is in the range of 0.75-0.80 [52,54]. Bionic texture [49] and self-adaptive texture [10] yielded high LCC than conventional grooves.

Table 5. Articles involving isothermal studies incorporating mass conserving algorithm.

Article	Input parameters	Findings
Fesanghary and Khonsari [11] 2010	JFO model, self-adaptive grooves Classic plate equation Foil thickness: 7- 15 μm Width/length: 1-100 l_r: 0.3-0.75	Self-adaptive grooves withstand more load than conventional grooves. 3% W increased by Width/length large ratios. Width/ l_r less than 10 should be used by the mass conserving model.
Zhang [3] 2012	JFO model, grooves N_g: 24; 24; 96 d: 4.6; 10.2; 5.2 μm Cavitation pressure: 10-90 kPa	JFO model under applied load 30 kPa obtained similar results with the experiment. Maximum values of the μ obtained by the Reynolds model were 71% of experimental values.
Sharma [59] 2014	JFO model, dimples Power law index: 0.9; 1; 1.1 The shape of dimples: Conical, Spherical	The hydrodynamic effect can improve by lubricants of the micro dimples.
Yagi et al. [60] 2015	JFO model, circular dimples d_r: 0.1-6, Diameter ratio: 0.1-0.9	W depends on D and d.
Feng and Peng [61] 2018	JFO model, grooves N_g: 60; 90; 120, d: 0-30 μm Groove angle: 4°, 2.7°, 2°, w_r: 0.1-0.9	Maximum W: 403 N, F: 29.26 N: w_r 0.667, N_g: 60, Groove angle 4°, d: 21 μm
Kumar et al. [62] 2019	JFO model, grooves d 0-0.06 mm, Angular width 0-10° Length of groove: 0-40 mm The shape of the groove: Circular, Triangular	Full section circular groove provides: 138.94% increment in W, 52.58% reduction of Frictional power Maximum W generated: Groove angular width 7.8°, d: 0.04 mm
Atwal and Pandey [65] 2020	JFO model, pocket Bearing pad: Plain, Pocket New textured	h_{min} increased: 19–48% with textured pad, 17–43% with pocketed pad μ reduced: 7–24% with texture pad, 6– 22% with pocketed pad At the mid-section of the pad, β of 0.7 gives the best performance.
Kumar et al. [64] 2020	JFO model, elliptical dimples Configurations of elliptical shape dimple: semi-minor and major axis in the x-direction, d_r: 0-1.6 Roughness parameter: 1/9-9	Maximum W: d_r 0.8 Elliptical dimple semi-major axis in the x-direction. Elliptical dimples reduce F by 48.3%.
Atwal et al. [63] 2021	JFO model, pocket New pocket, Rectangular pocket, Plain pad	Enhance h_{min}: 96–270% with new conceived pocketed pad and 85–232% with rectangular pocketed pad F reduced: 9–14% with new conceived pocketed and 8–12% with rectangular pocketed.
Fowell et al. [66] 2007	First-order Reynolds equation, pocket d: 5 μm K: 0-1	Pocket reduces friction: In the same proportion of surface area covered by it. Increasing load support By increasing h_{min}
Fowell et al. [67] 2012	Second-order Reynolds equation, pocket N_p: 2-30, β: 0-1, ρ_c: 0-100%	The textured area must begin in the first half of the bearing. d affected by h_{min}.
F.M. Meng [68] 2013	Second-order Reynolds equation, circular dimples d: 0-3 μm, l_r: 0.2-2	d increases: Increases F, Increases W
Almaida et al. [69] 2019	Swart Gelber Belamri (CFD), rectangular dimples, w: 0.5mm	Cavitation cannot be neglected to obtain accurate results for the bearing with texture.

3.2 Isothermal studies incorporating mass conserving algorithm

In the past, researchers working on textured bearing neglected cavitation and assumed pressure not to reach the sub-ambient zone. To make the solution more realistic, cavitation can't be neglected. When a non-textured surface (stator) moves with respect to a textured (runner) surface, it results in the formation of divergent and convergent zones in a thrust pad bearing. Low pressure exists in the divergent zone, which results in the suction of the lubricant from the vicinity. This leads to an increase in the flow rate of lubricant which enhances the magnitude of

hydrodynamic pressure [66,67]. Due to local pressure reduction below ambient pressure in the divergent zone of dimple or groove, cavitation of lubricant occurs which affects the performance of the thrust pad bearing. The Jakobson-Floberg-Olsson (JFO) cavitation model [3,11,37,57-65] is a widely used model by researchers. However, some researchers have used the first-order Reynolds equation [66-68] and CFD (using the Zwart Gelber Belamri model) [69] to incorporate cavitation.

Researchers revealed that film thickness is increased up to 270% [63,65] and friction coefficient reduced up to 24% [63-65] in the presence of textured surfaces, such as dimples [57-60,64,68], grooves [3,61-62], pockets [63,65-67] and self- adaptive grooves [11]. Various texture parameters considered are depth [3,57-58,60-66,68], width [61], and the shape of texture such as trapezoidal [57], square [58], conical [59], spherical [59], circular [62], elliptical [64] texture area density [57], number of dimples/grooves [3,61], the position of texture [57], texture extent [57-58,63,65,67], convergence ratio of pad [57,59,66-67]. Fesanghar**y** and Khonsari [11] introduced a bearing having a self-adaptive surface that has small grooves which can deform when the applied load is increased and provide a flexible surface texture. Reynolds equation is used for the computation of pressure and the classic plate equation is used for determining deformation. Zhang et al. [3] explored two cavitation models, the Reynolds model and the JFO model, and concluded that results obtained with the JFO model provide cavitation investigation nearly similar to the experimental results. A summary of the articles involving isothermal studies incorporating mass-conserving algorithms on textured pads is given in Table 5.

It can be concluded from Table 5 that cavitation cannot be neglected to obtain the accurate result of the performance of a textured bearing [3, 69]. The JFO model can express cavitation characteristics more closely than the Reynolds model [3]. The depth of the micro-geometries affects minimum film thickness [67] and LCC is improved when the depth of grooves is in the range of 21-40 μm [61,62] and the dimple depth ratio is 0.8 [64]. Pockets and textured pockets can improve the performance of bearing; minimum film thickness in the range of 48-270% [63,65] and coefficient of friction in the range of 14-24% [63,65]. Self-adaptive grooves withstand more load as compared to conventional grooves [11].

3.3 Numerical studies incorporating thermal effects without considering cavitation

Today, bearing speeds and loads have increased to a point where thermal effects need to be taken into consideration. The heat created in the lubricant film has a severe effect on the performance behaviour of bearings, therefore, the thermal effects need to be considered. The performance behaviour of bearing can be obtained using CFD simulations [70-75] based on the solution of Navier Stokes equation along with the energy equation for steady-state incompressible Newtonian fluid in laminar flow. Bearing performance parameters are affected by types of texture such as dimples [70-71], grooves [73], and pockets [72-74] and texture parameters such as depth [71-73], extent [71,73,75], the shape of texture such as grooves[62] and elliptical [75] circular. Fouflias et al. [72] investigated the performance behaviour of four types of thrust pad bearing namely, open pocket bearing, closed pocket bearing, tapered land bearing and partially textured employing rectangular dimples using computational fluid dynamics simulations. Results revealed that the performance of the bearing is affected by speed, film thickness, and texture depth. The best performance of bearing is attained in the presence of an open pocket. Different types of pockets are shown in Fig. 7.

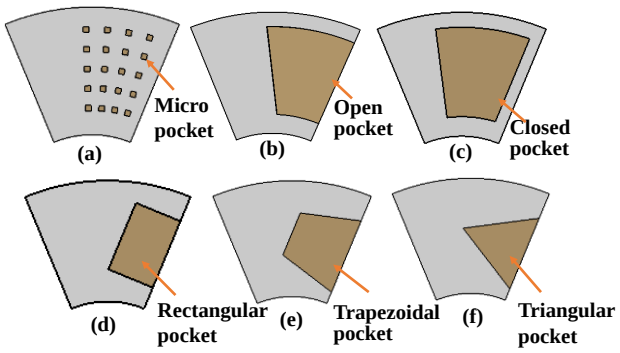

Fig. 7. Schematic illustration of different types of pockets (a) Micro-pockets (b) open pockets (c) closed-pocket. Different shapes of open-pocket (d) rectangular (e) Trapezoidal (f) Triangular.

It can be seen in Fig. 7 that a pocket can be a micro-pocket (where innumerable pockets are located on the pad) as shown in Fig. 7(a) and a macro-pocket or a large-sized pocket as shown in Fig. 7(b)-7(f). A pocket can be closed pocket (enclosed from all sides) or open (enclosed from 3 sides and open from the entry side). Different shapes of pockets are illustrated in Fig. 7(d)-7(f). A summary of articles involving numerical studies incorporating the thermal effects of textured pads without considering cavitation is provided in Table 6.

It can be observed from Table 6 that inlet texture increases LCC when thermal effects are considered [70]. It is revealed by researchers that the performance of bearing improved when the circumferential extent is 0.66 [71] and the radial extent in the range of 0.75-0.80 [71,74-75]. Open pockets improve load-carrying to the maximum extent [72]. Pocketed bearings improve the bearing performance more than grooved bearings [73]. Texture can reduce the pad surface temperature by 5-7^{0}C [73,75]. The best results are obtained for the cases when the dimple depth is equal to the minimum film thickness [71] whereas the depth of the pocket is 4-6 times [74] the minimum film thickness.

3.4 Numerical/ computational studies considering thermal as well as cavitation effects

Reynolds equation is used to compute pressure at different nodes in the domain in the lubricating film incorporating the cavitation model along with the energy equation. JFO cavitation model [2,8,77-80] is widely used in thermo-hydrodynamic lubrication. Performance parameters such as LCC and friction are affected by types of texture, namely, grooves [2], pockets [8,79-80] and texture parameters such as depth [2,76,78-79], texture area density [78], texture extent [78-79], width ratio [2] position [2], the shape of texture such as the square shape of grooves [2], square shape of pocket [77], trapezoidal shape of pockets [79]. The best geometry suggested by Aggarwal and Pandey [2] of the grooved textured pad is four grooves having a square cross-section of 30 μm depth**.**

Table 6. Articles involving numerical studies incorporating thermal effects without considering cavitation.

Article	Input parameters	Findings
Cupillard et al. [70] 2009	FVM, rectangular dimples K: 0-5, U: 0-40 m/s, d_r: 0.75	Dimples affected W : Speed and inlet flow rate were varied The convergence ratio is lower than 1
Papadopoulos et al. [71] 2013	FVM, rectangular dimples N: 1000-10000 rpm h_{min}: 20-100 μm, Dimple radial width: 9-19 mm, d: 10-40 μm, ρ_c: 30-70%, β: 0.22-0.77	W increases proportionally: with N The quadratic inverse of h_{min} W is maximum d=h_{min}
Fouflias et al. [72] 2014	FVM, pocket, dimples Open pocket, Closed pocket, Rectangular dimple textured, Tapered land bearing, h_{min}:10-80 μm, Re: 1-89, N: 2000-10000 rpm	W increases : The quadratic inverse of h_{min} Open-pocketed bearing having the highest value of W
Zouzoulas et al. [73] 2017	FVM, pocket, grooves, dimples N: 1500; 3000 rpm P_a: 0.5-2.5 MPa Plain bearing, Pocket, circumferential groove, radial grooves, rectangular dimple	Pocket and Circumferentially grooves: Improved h_{min} by 10–24% and 4–20% respectively Reduced maximum temperature by 7°C and 5.5°C respectively.
Charitopoulos et al. [74] 2018	FVM, pocket Two configurations were used: Taper land bearing, Curved pocket bearing N: 50000-250000 rpm	Improving the performance of bearing: β should be 0.8 d: 4–6 times h_{min} 40% h_{min} is increased and 12% power loss is decreased.
Fu and Untaroiu [75] 2018	FVM, dimples The shape of the dimple: Rectangular, Elliptical α: 0.5-0.9 β: 0.3-0.7	Elliptical dimples provide: Higher W The fluid film temperature is small The optimum β is 0.8 The optimum α of elliptical dimples is 30% larger than rectangular dimples. Maximum temperature reduces: 1.1% and 1.3% by rectangular and elliptical dimples respectively.

Table 7. Articles involving numerical simulations considering thermal as well as cavitation effect.

Article	Input parameters	Findings
Checo et al. [76] 2014	JFO model, dimples d: 0-10 μm	Best results obtained: texture width comparable to l. $d= 2*h_{min}$.
Aggarwal and Pandey [2] 2016	JFO model, grooves Different shapes of grooves (circular, trapezoidal, triangular, square) Different locations (entry, middle, exit, full surface)	$K\leq 0.25$. Grooves at entry side, square shape grooves: increased W up to 97%, reduced μ up to 51% Best geometry of textured pad : N_g: 4, the shape of the groove is square, d: 30 μm, w: 6.75mm
Aggarwal and Pandey [77] 2018	JFO model, pocket, dimples Different Pocket cross-sections (circular, square, trapezoidal, triangular) Different dimples (cylindrical, ellipsoidal, hemispherical) At different locations (entry, exit middle and full surface)	Square-shaped pocket toward the entry side contributes: increasing W, reducing μ.
Gropper [78] 2018	JFO model, rectangular dimples d: 9-47 μm α: 0.39-0.74, β: 0. 56-0.91 N: 1000; 2000 and 3000 rpm W: 0.5-2.0 MPa	At 0.75 β, h_{min} is maximum At 0.5 β, μ *is* minimum At 0.87 β, lowest maximum temperature. At 0.67 β, h_{min} and μ are high.
Atwal and Pandey [8] 2019	JFO model, pocket, bionic grooves Fish (Musa acuminate, Labeo Rohita, Thunnini, and Sailfish) Pocket, Fish scale texture, Pocketed fish textured	h_{min} increases by a combination of pocket and fish bionic texture 10–45%, pocket 10–42%; fish bionic texture 6–35% μ is reduced by 5-18% by Pocketed-fish textured among all the textured pads considered.
Atwal and Pandey [79] 2021	JFO model, pocket Tilted Pad Plain, rectangular pocket, trapezoidal rectangular pocket, Trapezoidal textured	h_{min} enhanced: 16–48% by combination of trapezoidal pocket and textured pad, 18–60% by trapezoidal pocketed pad Power loss reduced: By 4–10% with the combination of trapezoidal pocket and textured 5–13% with trapezoidal pocket Temperature reduced: 3–10% by the combination of trapezoidal pocket and textured 8–13% by trapezoidal pocket
Chalkiopoulos et al. [80] 2021	Rayleigh Plesset (CFD), grooves length: 3 mm, d: 4 mm	Performance of bearing is affected by thermal deformations: W reduced by 13% μ is increases by 10%.

Chesco et al. [76] indicated that the best results are obtained when the dimple depth is twice the clearance between the pad and the runner. A summary of the study of texture in articles involving numerical simulations considering thermal and cavitation effects is given below in Table 7. It can be concluded from Table 7 that the bearing performance is affected by thermal deformation [80]. The performance of the bearing is improved when the depth of the dimple is twice the film thickness [76] and the depth of the groove is 30 μm [2]. Square-shaped grooves [2] and pockets [77] at the inlet increase LCC and reduced friction coefficient and temperature. More lubricant enters at the entry of groove compared at the exit, which results in high pressure development in order to satisfy continuity law. Due to the temperature reduction and pressure generation, LCC increases [2,77]. The circumferential extent should be 0.66 to improve the performance of the bearing. Textured pockets increased minimum film thickness in the range of 10-60% [8,79] and reduced friction coefficient by 5-18% [8,79]. New techniques Fourier amplitude sensitivity test method [81] and machine learning [82] were introduced in recent research on surface texture. Geng et al. [81] introduced the Fourier amplitude sensitivity test method to calculate first-order sensitivity indices of parameters of texture. Zhu et al. [82] generated wavy and chevron dimples through machine learning reduced friction coefficient by 27-49% and increased load carrying capacity by 126-144% compared to design by conventional methods.

4. RESULTS AND DISCUSSION

Based on the investigations carried out by various researchers on the textured pad bearings, it is revealed that texture comprising micro-geometries such as dimples, grooves, pits or pockets improves the performance behaviours of the bearings. However, it is also noticed that the coefficient of friction and LCC depends on the texture parameters such as shape and depth of micro-geometries, texture extent, and textured area density. In this section, a comparison of the performance behaviours of pad thrust bearing incorporating different types of textures is discussed. Texture parameters for different micro-geometries are shown in Table 8.

Table 8. Texture parameters for different types of micro-geometries comprising texture.

Type of texture	Depth	Shape	Texture Parameter
Pits [27-30]	2-16.6 μm	Circular	D= 50-650 μm ρ_c =2.8-22.5
Dimples [12-15,17,32-36,38,41-44,46,48,50,53-55,59-60,64,68-73,75-78]	3-200 μm	Circle/ spherical, Rectangular/ square, triangle/ conical, trapezoidal, Elliptical	D= up to 800 μm ρ_c =0.1-0.80 d_r=0.001-1 w_r=0-1.2 N_d=1-100 α=0-1 β=0-1
Grooves [2,3,11,16,19,22-26,39,45,47,52,61-62,73,80]]	up to 100μm	Circular, Triangular, Trapezoidal, Square,	l: up to 40mm d_r=0.25-1.25 w_r=0.15-0.50 ρ_c =0.9 -0. 25 N_g= Up to 12 w= 100-2500 μm
Pockets [8,18,20,37,40,51,63,65-67,72-74,77,79]	0.01- 0.4 mm	Rectangular, Trapezoidal	D= 0.6-0.14mm β: 0-1 ρ_c =0-1

Researchers have used pits, grooves, pockets and dimples for the generation of texture on the pad surface. A comparison of the depth of pits, dimples, grooves and pockets is shown in Fig. 8. Pits are geometrical shapes which have an effective depth of 3.2 μm [27-30]. Dimples have an effective depth of 10 μm [16,32,44,48,76] which is three times that of pits. Grooves and pockets have an effective depth of 35 μm [2,25,49] and 40 μm [20,51] respectively. Local film thickness is increased in the presence of dimples/grooves. Higher local film thickness provides more LCC and also reduces metal-to-metal contact [47].

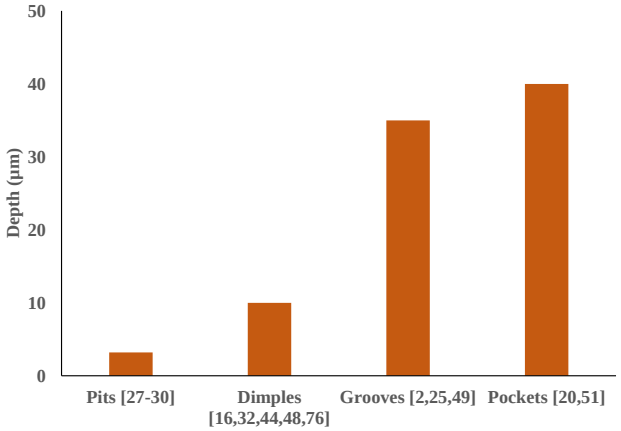

Fig. 8. Comparison of depth of pits, dimples, grooves and pockets.

The percentage reduction of friction torque using different shapes of dimples (cylindrical, elliptical, triangular and circular) in comparison to rectangular-shaped dimples is shown in Fig. 10. Researchers revealed that the cylindrical, elliptical, triangular and circular shapes of the dimple reduced friction torque respectively by more than 35% [77], 20% [44,75,77], 12% [41,44] and 6.25% [14,41,44,77] than rectangular dimples as shown in Fig. 9.

Effective parameters of dimples are also suggested by the researchers. The dimple depth ratio is the ratio of the depth of the dimple to the minimum film thickness. It is recommended by the researchers that the effective depth ratio is 0.8[52,54,64]. Texture area density is defined as the ratio of the dimple textured area to the cell area (containing the dimple). To improve the performance of the bearing 8% [32,44] texture

area density is suggested. A circumferential extent of 0.6 [18,43,78] and a radial extent of 0.8 [70,75] should be used for best performance. All these dimple parameters are shown in Fig. 10.

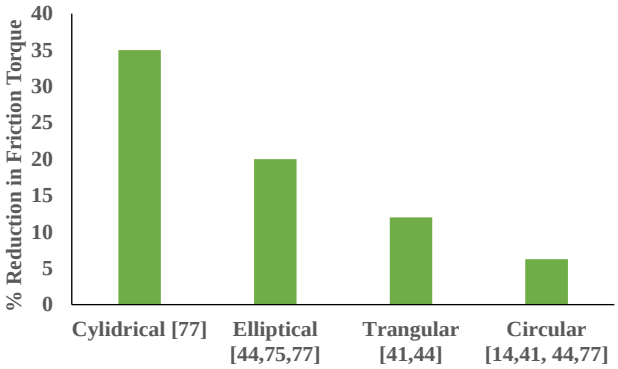

Fig. 9. Reduction in friction torque employing different shapes of dimples in comparison to rectangular shape dimples.

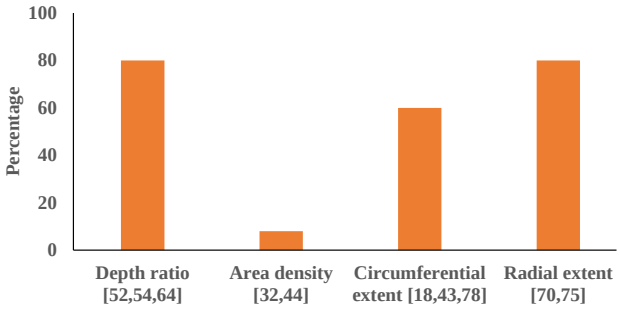

Fig. 10. Dimple parameters which yield maximum improvement in performance behaviours.

Performance improvement of pockets and grooves with respect to dimples has been compared and illustrated in Fig. 11. Researchers investigated the performance of pockets and grooves in comparison to dimples as shown in Fig. 11.

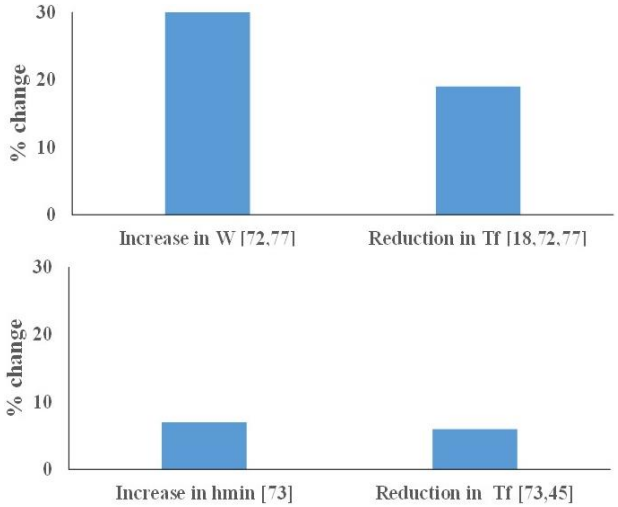

Fig. 11. Comparison of the performance of (a) pockets with respect to dimples, (b) grooves with respect to dimples.

It is noticed that pockets improve LCC by more than 30% [72,77] and reduced friction torque by more than 19% [18,72,77] compared to dimples. Grooves improve minimum film thickness by more than 7% [73] and reduced friction torque by more than 6% [73,45] in comparison to dimples. Therefore, it can be concluded that pockets and grooves improve the performance of the bearing more than dimples. Moreover, pockets out-performs grooves as it results in a higher reduction in friction torque in comparison to grooves.

5. CONCLUSION

Surface texture is employed to improve the performance of thrust pad bearings. Experimental and numerical studies reveal that partial texture towards the entry side improves the load capacity, and reduces friction coefficient and temperature rise of the pad. However, full surface texture deteriorates the performance. Also, the benefits of textured pads are realized at a lower convergence ratio (less than 1).

Performance behaviours of the pad thrust bearing also depend on texture parameters such as location, depth, width, shape and texture area density. Dimples located towards the inlet yield more favourable results in comparison to dimples located at other locations. The performance of the bearing is improved when the radial extent of the texture is in the range of 0.75-0.9 and the circumferential texture extent is 0.66. Different shapes of dimples are explored in order to study their effect on the performance of thrust pad bearing such as triangular, elliptical, rectangular, circular, square, trapezoidal, spherical and cylindrical. The cylindrical shape of the dimple yielded a maximum reduction in friction torque. Higher load-carrying is achieved when the depth of grooves is in the range of 21-40 μm and the dimple depth ratio is in the range of 0.75-0.8.

The presence of a pocket is more beneficial in terms of increasing minimum film thickness and reducing friction than a pad with dimples or grooves. Moreover, the grooved pad yields higher load-carrying and lower friction coefficient than pads with dimples. Self-adaptive and bionic textures improve the performance behaviour of thrust pad bearings as compared to conventional textures.

However, limited explorations are carried out on bionic textured and self–adaptive textured pads. As a part of future work, investigations of bionic texture and self-adaptive texture can be explored in order to improve performance behaviours. It is noticed that the texture parameters depend on operating conditions and pad geometry, therefore, further investigations and optimization can be carried out in this area. Most of the work related to surface texture is based on numerical/computational studies. Very few experimental studies on the thrust pad bearing test rig are conducted, therefore, computational investigations can be supported by experimental explorations.

REFERENCES

[1] M.M Khonsari, E.R. Booser, *Applied tribology; bearing design and lubrication*, John Wiley & Sons, Third edition, pp. 221-253, 2017, doi: 10.1002/9781118700280

[2] S. Aggarwal, R.K. Pandey, *Frictional and load-carrying behaviours of micro-textured sector shape pad thrust bearing incorporating the cavitation and thermal effects*, Lubrication Science, vol. 4, iss. 4, pp. 255-277, 2016, doi: 10.1002/ls.1367

[3] J. Zhang, Y. Meng, *Direct Observation of Cavitation Phenomenon and Hydrodynamic Lubrication Analysis of Textured Surfaces*, Tribology Letters, vol. 46, pp. 147–158, 2012, doi: 10.1007/s11249-012-9935-6

[4] D. Gropper, L. Wang, T. Harvey *Hydrodynamic lubrication of textured surface: A review of modelling techniques and key findings* Tribology International, vol. 94, pp. 509-529, 2016, doi: 10.1016/j.triboint.2015.10.009

[5] P. Lu. J.K. Robert, *Tribological performance of surface texturing in mechanical applications- A review*, Tribology Letters, vol. 8, 2020, doi: 10.1088/2051-672X/abb6d0

[6] K.H. Huebner, *A three-dimensional thermo hydrodynamic analysis of sector thrust bearings*. ASLE Transactions, vol- 17, iss. 1, pp. 62-73, 1974, doi: 10.1080/05698197408981439

[7] M.J. Braun, W.M. Hannon, *Cavitation formation and modelling for fluid film bearings: A review*, Proceeding of the Institution of Mechanical Engineers, Part J: Journal of Engineering Tribology, vol. 224, iss. 9, pp. 839-863, 2010, doi: 10.1243/13506501JET772

[8] J.C. Atwal, R.K. Pandey, *Performance analysis of thrust pad bearing using micro-rectangular pocket and bionic texture*, Proceeding of the Institution of Mechanical Engineers, Part J: Journal of Engineering Tribology, vol. 235, iss. 6, pp. 1232-1250, 2020, doi: 10.1177/1350650120940076

[9] Z. Xie, J. Jiao, K. Yangm H. Zhang, *A state of art review on the water lubricated*, Tribology International, vol. 180, 2023, doi: 10.1016/j.triboint.2023.108276

[10] R.Duvvuru, R.L Jackson, J.W. Hong, *Self-Adapting Micro scale Surface Grooves for Hydrodynamic Lubrication*, Tribology Transactions, vol. 52, iss. 1, pp. 1-11, 2016, doi: 10.1080/10402000801888960

[11] M. Fesanghary, M.M. Khonsari, *On Self-Adaptive Surface Grooves*, Tribology Transactions, vol. 53, iss. 6, pp. 871-880, 2016, doi: 10.1080/10402004.2010.496071

[12] I. Etsion, G. Halperin, V. Brizmer, Y. Kligerman, *Experimental investigation of laser surface textured parallel thrust bearings*, Tribology Letters, vol. 17, iss. 2, pp. 295–300, 2004, doi: 10.1023/B:TRIL.0000032467.88800.59

[13] S. Kawabata, S. Iwanami, T. Hotta, F. Itoigawa, T. Nakamura, *Hydrodynamic Lubrication Effects of Multiple Circular Bump Pattern for a Thrust Sliding Bearing of a Scroll Compressor*, Tribology Online, vol. 7, iss. 1, pp. 13–23, 2012, doi: 10.2474/trol.7.13

[14] N. Miyanaga, T. Kishida, J. Tomioka, *Experimental investigation of load carrying capacity and frictional torque of dimpled parallel thrust bearings,* Journal of advanced mechanical design, system and manufacturing, vol. 14, iss. 3, pp. 1–9, 2020, doi: 10.1299/jamdsm.2020jamdsm0041

[15] C. Changsheng, L. Shan, M. Zhenlai, L. Guoping, W. Qiang, *Study on the Influence of Surface Texture on the Dynamic Performance of Sliding Bearing*, Journal of physics: conference series, vol. 1820, 2021, doi: 10.1088/1742-6596/1820/1/012108

[16] S.B. Glavatskih, D.M.C. Mccarthy, I. Sherrington, *Hydrodynamic Performance of a Thrust Bearing with Micro patterned Pads*, Tribology Transactions, vol. 48, pp. 37–41, 2007, doi: 10.1080/05698190500313486

[17] Y. Henry, J. Bouyer, M. Fillon, *An experimental analysis of the hydrodynamic contribution of textured thrust bearings during steady state operation - Comparison with the untextured parallel surface configuration,* Proceeding of the Institution of Mechanical Engineers, Part J: Journal of Engineering Tribology, vol. 229, iss. 4, 2015, doi: 10.1177/1350650114537484

[18] Y. Henry, J. Bouyer, M. Fillon, *Experimental analysis of the hydrodynamic during start-up of fixed pad thrust bearing*, Tribology International, vol. 120, no. 4, pp. 299–308, 2018, doi: 10.1016/j.triboint.2017.12.021

[19] T. Chen, J. Ji, Y. Fu, P. Tian, *Tribological analysis of picosecond laser partially textured thrust bearings with circular grooves machined: Theory and experiment*, Proceeding of the Institution of Mechanical Engineers, Part J: Journal of Engineering Tribology, vol. 235, iss. 1, pp. 105-122, 2021, doi: 10.1177/13506501211005873

[20] J. Bouyer, M. Wodtke, M. Fillon, *Experimental research on a hydrodynamic thrust bearing with hydrostatic lift pockets: Influence of lubrication modes on bearing performance*, Tribology International, vol. 165, pp. 80-233, 2022, doi: 10.1016/j.triboint.2021.107253

[21] A.M. Mikula, *The Leading-Edge-Groove Tilting-Pad Thrust Bearing: Recent Developments*, ASME Journal of Engineering Tribology, vol. 107, iss. 3, pp. 423-428, 1985, doi: 10.1115/1.3261099

[22] M. Fesanghary, M.M. Khonsari, *On the optimum groove shapes for load-carrying capacity enhancement in parallel flat surface bearings: Theory and experiment*, Tribology International, vol. 67, pp. 254–262, 2013, doi: 10.1016/j.triboint.2013.08.001

[23] M.D. Ibrahim, Y. Sunami, S.S. Lam, *Characteristics of modified spiral thrust bearing through geometries and dimension modification*, Tribology Online, vol. 13, iss. 6, pp. 334–339, 2018, doi: 10.2474/trol.13.334

[24] Y. Hu, Y. Meng, *Theoretical and experimental study of transient behaviour of spiral-grooved thrust bearings during start-up* Tribology Transactions, vol. 63, iss. 1, pp. 154-172, 2019, doi: 10.1080/10402004.2019.1670887

[25] X. Gan, *Research on the performance of water-lubricated hydrodynamic spiral groove thrust bearing,* Conference paper: Earth and environment science, vol. 632, 2021, doi: 10.1088/1755-1315/632/5/052005

[26] X. Lin, *Study on Static Characteristics of Water-Lubricated Textured Spiral Groove Thrust Bearing Using Laminar Cavitating Flow Lubrication Model*, ASME Journal of Tribology, vol. 144, iss. 4, pp. 1–13, 2022, doi: 10.1115/1.4051655

[27] X. Wang, *The effect of laser texturing of SiC surface on the critical load for the transition of water lubrication mode from hydrodynamic to mixed*, Tribology International, vol. 34, iss. 10, pp. 703–711, 2001, doi: 10.1016/S0301-679X(01)00063-9

[28] X. Wang, K. Kato, K. Adachi, K. Aizawa, *Loads carrying capacity map for the surface texture design of SiC thrust bearing sliding in water*, Tribology International, vol. 36, iss. 3, pp. 189–197, 2003, doi: 10.1016/S0301-679X(02)00145-7

[29] P. Taylor, X. Wang, K. Kato, K. Adachi, *The Lubrication Effect of Micro-Pits on Parallel Sliding Faces of SiC in Water*, Tribology Transactions, vol. 45, iss. 3, pp. 294-301, 2008, doi: 10.1080/10402000208982552

[30] X. Wang, W. Liu, F. Zhou, D. Zhu, *Preliminary investigation of the effect of dimple size on friction in line contacts*, Tribology International, vol. 42, iss. 7, pp. 1118–1123, 2009, doi: 10.1016/j.triboint.2009.03.012

[31] Y. Lu, *The Biomimetic Shark Skin Optimization Design Method for Improving Lubrication Effect of Engineering Surface*," Proceeding of the Institution of Mechanical Engineers, Part J: Journal of Engineering Tribology, vol. 136, iss. 3, pp. 1–13, 2014, doi: 10.1115/1.4026972

[32] H. Zhang, D. Y. Zhang, M. Hua, G.N. Dong, K.S. Chin, *A Study on the Tribological Behaviour of Surface Texturing on Babbitt Alloy under Mixed or Starved Lubrication*, Tribology Letters, vol. 56, pp. 305–315, 2014, doi: 10.1007/s11249-014-0410-4

[33] A. Ancona, G.S. Joshi, A. Volpe, P. Mario, G. Carbone, *Non-Uniform Laser Surface Texturing of an Un-Tapered Square Pad for Tribological Applications*, Lubricants, vol. 5, iss. 4, pp. 1–13, 2017, doi: 10.3390/lubricants5040041

[34] M. Taee, A. Torabi, S. Akbarzadeh, *On the Performance of EHL Contacts with Textured Surfaces*, Tribology Letters, vol. 65, pp. 65-85, 2017, doi: 10.1007/s11249-017-0871-3

[35] Q. Dai, Q. Chang, M. Li, W. Huang, X. Wang, *Non-sticky and Non-slippery Bionic Patterned Surfaces*, Journal of Bionic Engineering, vol. 17, pp. 326–334, 2020, doi: 10.1007/s42235-020-0026-3

[36] H. Yu, H. Deng, W. Huang, X. Wang, *The effect of dimple shapes on friction of parallel surfaces*, Proceeding of the Institution of Mechanical Engineers, Part J: Journal of Engineering Tribology, vol. 225, iss. 8, pp. 693–703, 2015, doi: 10.1177/1350650111406045

[37] Y. Mao Z. Yin, *Modelling and experiments of cavitation on a pocket-textured surface*, Proceeding of the Institution of Mechanical Engineers, Part J: Journal of Engineering Tribology, vol. 234, iss. 1, pp. 94-103, 2019, doi: 10.1177/1350650119855903

[38] K. Yagi, W. Takedomi, H. Tanaka, J. Sugimura, *Improvement of Lubrication Performance by Micro Pit Surfaces*, Tribology Online, vol. 3, iss. 5, pp. 285–288, 2008, doi: 10.2474/trol.3.285

[39] T. Hirayama, H. Shiotani, K. Yamada, N. Yamashita, T. Matsuoka, *Hydrodynamic Performance Produced by Nano texturing in Sub micrometre Clearance with Surface Roughness*, Proceeding of the Institution of Mechanical Engineers, Part J: Journal of Engineering Tribology, vol. 137, iss. 1, pp. 1–3, 2015, doi: 10.1115/1.4028736

[40] A. Zavos, *The effect of square-shaped pockets position in sliding line contacts under mixed regime of lubrication*, Proceeding of the Institution of Mechanical Engineers, Part J: Journal of Engineering Tribology, vol. 233, iss. 3, pp. 490-506, 2018, doi: 10.1177/1350650118787625

[41] D.K. Panigrahi, *Tribological performance of positive deterministic textured surfaces in parallel sliding lubricated contacts: Effect of texture size and height*, Proceeding of the Institution of Mechanical Engineers, Part J: Journal of Engineering Tribology, vol. 234, iss. 12, pp. 1908-1934, 2020, doi: 10.1177/1350650119897479

[42] S.M. Hsu, Y. Jing, F. Zhao, *Self-adaptive surface texture design for friction reduction across the lubrication regimes*, Surface Topography: Metrology and Properties, vol. 4, no. 1, 2016, doi: 10.1088/2051-672X/4/1/014004

[43] V. Brizmer, Y. Kligerman, I.E.F. Stle, *A laser surface textured parallel thrust bearing*, Tribology Transactions, vol. 46, iss. 3, pp. 397–403, 2003, doi: 10.1080/10402000308982643

[44] H. Yu, E.X. Wang, E.F. Zhou, *Geometric Shape Effects of Surface Texture on the Generation of Hydrodynamic Pressure between Conformal Contacting Surfaces*, Tribology Letters, vol. 37, pp. 123–130, 2010, doi: 10.1007/s11249-009-9497-4

[45] S. Aggarwal, R.K. Pandey, *Combined effects of grooves and dimpling on the performance parameters of sector-shaped pad thrust bearings* Conference on Industrial Tribology, in National Tribology Conference NTC, 15 – 17 December, 2014, PES UNIVERSITY, Bengaluru, India.

[46] K. Yagi, J. Sugimura, *Performance of Balancing Wedge Action in Textured Hydrodynamic Pad Bearings,* ASME Journal of Tribology, vol. 139, iss. 1, pp. 1–11, 2017, doi: 10.1115/1.4033128

[47] M. Kouider, S. Dominique, Z. Djallel, Y. Abdelkader, *Effects of the dimple geometry on the isothermal performance of a hydrodynamic textured tilting- pad thrust bearing*, International Journal of Heat and Technology, vol. 36, no. 2, pp. 463–472, 2018, doi: 10.18280/ijht.360211

[48] H. Zhang, Y. Liu, M. Hafezi, M. Hua, G. Dong, *A distribution design for circular concave textures on sectorial thrust bearing pads*, Tribology International, vol. 149, 2019, doi: 10.1016/j.triboint.2019.04.017

[49] Y. Yu, G. Pu, T. Jiang, K. Jiang, *A dragonfly wing inspired bionic aerodynamic thrust bearing for increased load capacity*, International Journal of Mechanical Sciences, vol. 176, 2020, doi: 10.1016/j.ijmecsci.2020.105550

[50] F. Zeng, Y. Cheng, Z. Wan, Z. Long, Z. Zhang, Y. Tang, *Tribological Performance of Convex Compound Texture Under Hydrodynamic Lubrication*, ASME Journal of Tribology, vol. 144, iss. 4, pp. 1–10, 2022, doi: 10.1115/1.4051732

[51] A.D. Gosman, E. Ioannides, H.A. Spikes, *CFD Analysis of a Low Friction*, ASME Journal of Tribology, vol. 127, iss. 4, pp. 803–812, 2005, doi: 10.1115/1.2032990

[52] S.B. Glavatskih, R. Larsson, *Two-Dimensional CFD-Analysis of Micro-Patterned Surfaces in Hydrodynamic Lubrication*," ASME Journal of Tribology, vol. 127, iss. 1, pp. 96-102, no. January, 2005, doi: 10.1115/1.1828067

[53] M.J. Cervantes, *Pressure Build-up Mechanism in a Textured Inlet of a Hydrodynamic*, ASME, Journal of Tribology, vol. 130, iss. 2, pp. 1–10, 2008, doi: 10.1115/1.2805426

[54] J. Han, L. Fang, J. Sun, *Hydrodynamic Lubrication of Micro dimple Textured Surface Using Three-Hydrodynamic Lubrication of Micro dimple Textured*, Tribology Transactions, vol. 53, iss. 6, pp. 860-870, 2010, doi: 10.1080/10402004.2010.496070

[55] Y. Sun, S. Xu, T. Kyoizumi, K. Shimada, *CFD Analysis of Friction-Reduction Effect of Micro-Textured Surfaces in Lubricant*, International Journal of Automation Technology, vol. 12, no. 2, 2018, doi: 10.20965/ijat.2018.p0206

[56] A.G. Charitopoulos, E.E. Efstathiou, C.I. Papadopoulos, P.G. Nikolakopoulos, L. Kaiktsis, *Effects of manufacturing errors on tribological characteristics of 3-D textured micro- thrust bearings*, CIRP Journal of Manufacturing Science and Technology, vol. 6, iss. 2, pp. 128–142, 2013, doi: 10.1016/j.cirpj.2012.12.001

[57] M.B. Dobrica, M. Fillon, M.D. Pascovici, T. Cicone, *Optimizing surface texture for hydrodynamic lubricated contacts using a mass-conserving numerical approach*, Proceeding of the Institution of Mechanical Engineers, Part J: Journal of Engineering Tribology, vol. 224, iss. 8, pp. 737-750, 2010, doi: 10.1243/13506501JET673

[58] A. Gherca, A. Fatu, M. Hajjam, P. Maspeyrot, *Effect of surface texturing in steady state and transient flow condition: Two dimensional numerical simulation using a mass conserving cavitations*, Proceedings of the Institution of Mechanical Engineers, Part J: Journal of Engineering Tribology, vol. 229, iss. 4, pp. 509-522, 2014, doi: 10.1177/1350650114546432

[59] S.C. Sharma, S.K. Yadav, *Performance analysis of a fully textured hybrid circular thrust pad bearing system operating with non-Newtonian lubricant*, Tribology International, vol. 77, pp. 50–64, 2014, doi: 10.1016/j.triboint.2014.04.013

[60] K. Yagi, H. Sato, J. Sugimura, *On the Magnitude of Load-Carrying Capacity of Textured Surfaces in Hydrodynamic Lubrication*, Tribology Online, vol. 10, iss. 3, pp. 232–245, 2015, doi: 10.2474/trol.10.232

[61] H. Feng, L. Peng, *Numerical analysis of water-lubricated thrust bearing with groove texture considering turbulence and cavitation*, Industrial Lubrication and Tribology, vol. 70, iss. 6, 2018, doi: 10.1108/ILT-07-2017-0204

[62] V. Kumar, *Influence of micro-groove attributes on frictional power loss and load-carrying capacity of hybrid thrust bearing*, Industrial Lubrication and Tribology, vol. 72, iss. 5, pp. 589–598, 2020, doi: 10.1108/ILT-07-2019-0278

[63] J.C. Atwal, R.K. Pandey, *Performance improvement of water-lubricated thrust pad bearing operating with the turbulent flow using a new micro-pocket design*, Tribology International, vol. 154, 2020, p. 106738, 2021, doi: 10.1016/j.triboint.2020.106738

[64] V. Kumar, *Performance analysis of rough surface hybrid thrust bearing with elliptical dimples*, Proceeding of the Institution of Mechanical Engineers, Part J: Journal of Engineering Tribology, vol. 235, iss. 6, pp. 1101-1113, 2020, doi: 10.1177/1350650120931981

[65] J.C. Atwal, R.K. Pandey, *Film Thickness and Friction Investigations in a Fluid Film Thrust Bearing Employing a New Conceived Micro-Texture on Pads*, ASME Journal of Tribology, vol. 143, iss. 6, 2021, doi: 10.1115/1.4048500

[66] A.V. Olver, M.T. Fowell, H.A. Spikes, *Entrainment and Inlet Suction: Two Mechanisms of Hydrodynamic Lubrication in,* ASME Journal of Tribology, vol. 129, iss. 2, pp. 336–347, 2007, doi: 10.1115/1.2540089

[67] M.T. Fowell, S. Medina, A.V. Olver, H.A. Spikes, I.G. Pegg, *Parametric study of texturing in convergent bearings*, Tribology International, vol. 52, pp. 7–16, 2012, doi: 10.1016/j.triboint.2012.02.013

[68] F.M. Meng, *On influence of cavitation in lubricant upon tribological performances of textured surfaces*, Optics and Laser Technology, vol. 48, pp. 422–431, 2013, doi: 10.1016/j.optlastec.2012.10.020

[69] N. Almaida, M.R. Prasetyaji, M.H. Mafian, A.R. Hakim, *Cavitation modelling effect on pressure distribution of inclined lubricated contacts and textured surfaces using CFD*, Journal Tribologi, vol. 22, 2018, pp. 40–48, 2019.

[70] S. Cupillard, S. Glavatskih, M.J. Cervantes, *3D thermo hydrodynamic analysis of a textured slider*, Tribology International, vol. 42, iss. 10, pp. 1487–1495, 2009, doi: 10.1016/j.triboint.2009.05.021

[71] C. Papadopoulos, L. Kaiktsis, M. Fillon, *CFD Thermo hydrodynamic Analysis of 3-D Sector-Pad Thrust Bearings With rectangular dimples*, Conference on Turbo Expo power for Land Sea and Air American Society of Mechanical Engineers, June 3–7, 2013, San Antonio, Texas, USA, doi: 10.1115/GT2013-94043

[72] D.G. Fouflias, A.G. Charitopoulos, C.I. Papadopoulos, L. Kaiktsis, M. Fillon, *Performance comparison between textured, pocket, and tapered-land sector-pad thrust bearings using computational fluid dynamics thermo hydrodynamic analysis,* Journal of Mechanical Engineering, vol. 229, iss. 4, pp. 376–397, 2016, doi: 10.1177/1350650114550346

[73] V. Zouzoulas, C.I. Papadopoulos, *3-D thermohydrodynamic analysis of textured, grooved, pocketed and hydrophobic pivoted-pad thrust bearings*, Tribology International, vol. 110, pp. 426–440, 2017, doi: 10.1016/j.triboint.2016.10.001

[74] A.G. Charitopoulos, R. Visser, R. Eling, C.I. Papadopoulos, *Design Optimization of an Automotive Turbocharger Thrust Bearing Using a CFD-Based THD Computational Approach*, Lubricants, vol. 6, iss. 1, pp. 1–21, 2018, doi: 10.3390/lubricants6010021

[75] G. Fu, A. Untaroi, *The Influence of Surface Patterning on the Thermal Properties of Textured Thrust Bearings*, ASME Journal of Tribology, vol. 140, iss. 6, pp. 1–10, 2018, doi: 10.1115/1.4040383

[76] H.M. Checo, A. Jaramillo, M. Jai, G.C. Buscaglia, *Texture-induced cavitation bubbles and friction reduction in the Elrod – Adams model,* Journal of International Tribology, vol. 229, iss. 4, pp. 1–15, 2014, doi: 10.1177/1350650114550012

[77] S. Aggarwal, R.K. Pandey, *Performance investigation of micro-pocketed textured pad thrust bearing*, Industrial Lubrication and Tribology, vol. 70, iss. 8, pp. 1388-1395, 2019, doi: 10.1108/ILT-10-2017-0302

[78] D. Gropper, T.J. Harvey, L. Wang, *Numerical analysis and optimization of surface textures for a tilting pad thrust bearing*, Tribology International, vol. 124, pp. 134–144, 2018, doi: 10.1016/j.triboint.2018.03.034

[79] J.C. Atwal, R.K. Pandey, *Influence of new surface micro-structures on the performance behaviours of fluid film tilting pad thrust bearings*, Proceeding of the Institution of Mechanical Engineers, Part J: Journal of mechanical engineering science, vol. 6, iss. 6, pp. 3111-3134, 2021, doi: 10.1177/09544062211030972

[80] M. Chalkiopoulos, A. Charitopoulos, M. Fillon, C.I. Papadopoulos, *Effects of thermal and mechanical deformations on textured thrust bearings optimally designed by a THD*, Tribology International, vol. 148, 2020, doi: 10.1016/j.triboint.2020.106303

[81] Y. Geng, M. Lou, H. Liu, S. Qi, Y. Liu, W. Chen, *Global sensitivity analysis of hydrodynamic lubrication performance for textured surface*, Tribology International, vol. 177, 2023, doi: 10.1016/j.triboint.2022.107987

[82] B. Zhu, W. Zhang, W. Zhang, H. Li, *Generative design of texture for sliding surface based on machine learning*, Tribology International, vol. 179, doi: 10.1016/j.triboint.2022.108139

Nomenclature

A_C	Texture cell area (μm²)
$A_{texture}$	Texture area (μm²)
B	Width of the slider (μm)
D	Diameter of texture (μm)
d	Depth of texture (μm)
F	Friction force(N)
d_r	Depth ratio (d/h_{min})
h_1	Film thickness at entry edge (μm)
h_{min}	Minimum film thickness (μm)
K	Convergence ratio ((h_1/ h_{min})-1)
L	Length of slider(μm)
l	Length of pad(μm)
l_r	Length ratio (w/l)
N_d	Number of dimples
N_g	Number of grooves
N_p	Number of pockets
N	Rotational speed (rpm)
P_a	Contact pressure (Pa)
R_e	Reynolds number
S	Spacing between two dimples (μm)
U	Sliding velocity of runner (m/sec)
W	Load carrying capacity (N)
W_a	Applied load (N)
W	Width of dimple (μm)
w_r	Width ratio (w/s)
ρ_c	Texture area density ((A_C / $A_{texture}$)X100)(%)
A	Texture extent in radial direction
B	Texture extent in circumferential direction
μ	Coefficient of friction
T_f	Friction torque (Nm)